CrystEngComm

PAPER

View Article Online
View Journal

Cite this: DOI: 10.1039/d3ce00302g

Construction of Cd(II)-based metal–organic frameworks incorporating SiF_6^{2-} as fluorescence sensors for arginine†

Xue Wu,[a] Ding Li,[a] Lei Xu,[b] Yu-Fei Jiang,[a] Yue Zhao *[a] and Jing Zhao *[a]

Received 29th March 2023,
Accepted 27th April 2023

DOI: 10.1039/d3ce00302g

rsc.li/crystengcomm

Recently, the detection of amino acids has attracted considerable attention in the field of nutrition analysis, health monitoring, and medical diagnosis due to their significance for organisms. In this work, two novel Cd(II)-based metal–organic frameworks (MOFs) with the formulas $[Cd(bib)_2(SiF_6)]_n$ (**1**) and $\{[Cd(bib)_2(SiF_6)]\cdot DMF\cdot 3H_2O\}_n$ (**2**, bib = 1-(4-imidazol-1-ylphenyl)imidazole) were synthesized and exhibited fluorescence sensing capacity for arginine. In spite of having the same framework composition, complexes **1** and **2** showed great differences in their structure originating in the variations between the coordination modes of SiF_6^{2-} with Cd^{2+} and the extension direction of the Cd-bib coordination complexes. Structural analysis manifested that complex **1** featured a 3D coordination framework constructed from 2D Cd-bib coordination layers bridged by SiF_6^{2-} anions, while complex **2** possessed 3-fold interpenetrated Cd-bib coordination networks connected by SiF_6^{2-} anions. Furthermore, fluorescence sensing experiments exhibited that both complexes **1** and **2** could be used as fluorescence probes for arginine and the emission intensities of complexes **1** and **2** could be enhanced up to 10.3 and 12.0 times that of the initial emission intensities upon the addition of Arg, respectively.

Introduction

As the essential building units of proteins and enzymes, amino acids are indispensable to maintaining normal life activities and play an important role in various physiological processes. Both an excessive intake or lack of amino acids can cause side effects to human health or even serious diseases and thus an abnormal level of amino acids is usually regarded as a signal of some diseases.[1] On the other hand, the contents of amino acids are also an important indicator to evaluate the nutritional value of foods because the essential amino acids cannot be manufactured by the human body and must be taken in from the daily diet.[2] Therefore, the selective detection of amino acids is of great significance for nutrition analysis, health monitoring, and medical diagnosis.[3–9] Among all the natural amino acids, arginine (Arg) is the most basic one containing the guanidine group and is classified as a semi-essential or conditionally essential amino acid. Infants or young children cannot synthesize Arg in their bodies, which makes it nutritionally essential in infant formula and baby foods.[10] In addition, Arg is also involved in various metabolic processes or functions, including ammonia detoxification, regulating hormone secretion, maintaining the stability of blood pressure and the immune system, and the formation of urea, ornithine, nitric oxide, and agmatine.[11–20] Particularly, it has also been demonstrated that the content of Arg in human bodies has a high correlation with some diseases, such as anaphylaxis, blood ammonia imbalance, endothelium dysfunction, chronic pancreatitis, and cellular damage.[21–27] Moreover, some studies reported that the content of Arg is obviously lower than the normal level when breast, colon, pancreatic, *et al.* tumor cells emerge.[10,28] More recently, Alessandra and co-workers also reported a negative correlation between the plasma arginine level and the severity of COVID-19.[29] Thus, the content of Arg is recognized as one of the diagnostic indicators for many diseases. Therefore, the development of methods for the recognition of Arg has attracted numerous attentions and various methods have been exploited for the detection of Arg in the past several decades, among which the fluorescence sensing method has aroused particular interest in recent years due to its advantages of low cost, simple operation, high sensitivity, and quick response.[30–34]

[a] *Coordination Chemistry Institute, State Key Laboratory of Coordination Chemistry, School of Chemistry and Chemical Engineering, Nanjing University, Nanjing 210023, China. E-mail: zhaoyue@nju.edu.cn, Jingzhao@nju.edu.cn; Tel: +86 25 89681957*

[b] *Jiangsu Key Lab of Data Engineering and Knowledge Service, School of Information Management, Nanjing University, Nanjing 210023, China*

† Electronic supplementary information (ESI) available: PXRD, TG, IR spectra and additional figures. CCDC 2249374 and 2249375. For ESI and crystallographic data in CIF or other electronic format see DOI: https://doi.org/10.1039/d3ce00302g

Metal–organic frameworks (MOFs) are porous crystalline materials obtained by the self-assembly of metal ions or clusters with organic ligands and have been widely investigated in diverse fields, including gas adsorption/separation, catalysis, energy storage/conversion, drug delivery, chemical sensing, and so on due to their structural diversity, high porosity, large specific surface area, and easy modification.[35–39] Compared with other fluorescence materials, the fluorescence properties of MOFs could be readily regulated through the rational design of the organic ligands, selection of metal centers, post-synthetic modification, guest molecules exchange, and so on.[40–42] Hence, fluorescent MOFs have displayed great potential in the directional construction of sensing platforms and have exhibited the capacity to detect different substances or parameters, such as gas molecules, volatile organic compounds, nitro explosives, metal cations, inorganic anions, biomolecules, pH, and temperature.[43–47] Simultaneously, employing MOF-based sensing materials to identify Arg has also attracted considerable attention and seen inspiring achievements in the past several years. For instance, Yin and co-workers designed a dual-emission fluorescent Eu-MOF originating from the coordination-induced emission of the ligand 2,3,5,6-tetrakis(4-carboxyphenyl)pyrazine and antenna-effect emission of Eu^{3+} to realize the ratiometric fluorescence detection of Arg.[48] In addition, Hu *et al.* employed 2′,5′-dimethoxytriphenyl-4,4″-dicarboxylic acid as the organic linker to obtain four new isostructural lanthanide-based MOFs and the Eu/Tb-based MOFs exhibited a recognition capacity for Arg and lysine (Lys).[49] Moreover, Wang and co-workers synthesized four novel uranyl-based MOFs and two of them could be used as fluorescent sensors for Arg in aqueous media through the "turn-on" effect.[50] According to previous studies, d^{10}-metal-based MOFs usually possess satisfying fluorescence properties and thus have been widely investigated as fluorescent sensors.[51–53] However, to the best of our knowledge, the use of d^{10}-metal-based MOFs has been scarcely reported for the fluorescence sensing of Arg.

In consideration of the fact that imidazole-containing ligands have high flexibility, diversity, and a strong coordination capability to construct MOFs[54–57] and the potential of the SiF_6^{2-} anion to form hydrogen bonds, an imidazole-containing ligand 1-(4-imidazol-1-ylphenyl) imidazole (bib) was employed to react with $CdSiF_6$ to obtain two novel MOFs with the formulas of $[Cd(bib)_2(SiF_6)]_n$ (**1**) and $\{[Cd(bib)_2(SiF_6)]\cdot DMF\cdot 3H_2O\}_n$ (**2**). According to the single-crystal X-ray diffraction (SC-XRD) analysis, the distinction of the coordination modes of SiF_6^{2-} with Cd^{2+} and the extension direction of the Cd-bib coordination complexes resulted in a great difference in the structures between complexes **1** and **2** although they both had the same framework composition. Complex **1** featured a 3D non-porous coordination network constructed from the Cd-bib coordination layers and SiF_6^{2-} anions, while complex **2** displayed a 3D porous coordination framework built from the 3-fold interpenetrated bib-Cd coordination networks connected by SiF_6^{2-} anions. Moreover, both complex **1** and **2** could be used as selective fluorescent sensors for Arg through the "turn-on" effect.

Experimental

Materials and methods

All the utilized reagents and solvents were commercially purchased and used as received without further purification. The organic ligand bib was synthesized according to the previously reported procedure.[58] FT-IR spectra were recorded in the range of 400–4000 cm^{-1} using KBr pellets on a Bruker Vector 22 FT-IR spectrophotometer. Powder X-ray diffraction (PXRD) data were collected at room temperature on bulk samples with Cu Kα radiation (1.54059 Å) on a Bruker D8 Advance X-ray diffractometer. Thermogravimetric analyses (TGA) were carried out on a Mettler-Toledo (TGA/DSC1) thermal analyzer under nitrogen with a heating rate of 10 °C min^{-1} in the range of 30–800 °C. Fluorescence spectra were measured on a Perkin Elmer LS-55 fluorescence spectrometer. UV-vis measurements were collected at room temperature on a Shimadzu UV3600 spectrophotometer. The morphology and microstructural observations were carried out by field emission scanning electron microscopy (Hitachi S-4800) at an acceleration voltage of 5 kV.

Preparation of $[Cd(bib)_2(SiF_6)]_n$ (1). The DMF solution of bib (10.6 mg, 0.05 mmol, 4 mL) was carefully layered on the aqueous solution of $CdSiF_6$ (25.4 mg, 0.1 mmol, 4 mL) in a 10 mL glass tube and allowed to stand at room temperature without disturbance. After one week, colorless crystals of **1** could be obtained in a 25–30% yield. Anal. calcd for **1** ($C_{24}H_{20}CdF_6N_8Si$): C, 40.43%; H, 4.15%; N, 15.72%. Found: C, 40.64%; H, 4.05%; N, 15.83%. IR (KBr pellet, cm^{-1}, Fig. S4, ESI†): 3489 (br), 3121 (s), 1636 (m), 1525 (s), 1492 (m), 1308 (m), 1268 (m), 1246 (m), 1133 (m), 1103 (w), 1069 (s), 961 (m), 935 (m), 832 (m), 741 (s), 645 (m), 536 (w), 484 (m).

Preparation of $\{[Cd(bib)_2(SiF_6)]\cdot DMF\cdot 3H_2O\}_n$ (2). The preparation of complex **2** was similar to that of **1** except that the amount of $CdSiF_6$ was doubled to 50.8 mg (0.2 mmol). Colorless crystals of **2** were obtained in a 30–40% yield. Anal. calcd for **1** ($C_{27}H_{33}CdF_6N_9O_4Si$): C, 42.71%; H, 2.99%; N, 16.60%. Found: C, 42.34%; H, 3.05%; N, 16.83%. IR (KBr pellet, cm^{-1}, Fig. S4, ESI†): 3486 (br), 3121 (s), 1636 (m), 1532 (s), 1492 (m), 1308 (m), 1268 (m), 1246 (m), 1132 (m), 1102 (w), 1070 (s), 961 (m), 935 (m), 834 (m), 749 (s), 647 (m), 537 (w), 484 (m).

Fluorescence sensing experiments

Before the fluorescence experiments, the prepared crystal samples of complexes **1** and **2** were fully ground and dispersed in deionized water under ultrasonic treatment to prepare a steady suspension (1.0 mg mL^{-1}). Then, the excitation and emission spectra of the suspensions of **1** and **2** were measured at room temperature and their fluorescence sensing performance was examined by recording the emission bands after the addition of the solutions of different amino acids. The suspensions were all stirred at a constant rate during the fluorescence measurements for ensuring homogeneity and each experiment was repeated three times to obtain reliable data.

Quantitative titration and anti-interference experiments

In order to investigate the sensing sensitivity of complexes **1** and **2**, quantitative titration experiments were conducted by the gradual addition of Arg solution into the aqueous suspension of complexes **1** and **2**, and the fluorescent emission spectra were immediately recorded after the addition of Arg. Moreover, anti-interference experiments were carried out by the addition of the solutions of other amino acids and Arg into the suspension of complexes **1** and **2** in sequence. Every experiment was repeated three times to obtain reliable data.

Results and discussion

Crystal structure description

Crystal structure of complex 1. SC-XRD measurements revealed that complex **1** was crystallized in the monoclinic *C*2/*c* space group and its asymmetric unit consisted of one bib ligand, one-half Cd^{2+} cation, and one-half SiF_6^{2-} anion. As exhibited in Fig. 1a, atom Cd1 adopted a distorted octahedral coordination geometry to coordinate with four nitrogen atoms (N1#1, N1#2, N4, N4#1) from four different bib ligands and two fluorine atoms (F1, F1#1) from two adjacent SiF_6^{2-} anions. Each organic ligand bib connected two Cd^{2+} cations and each Cd^{2+} cation was bound to four different bib ligands, which generated two-dimensional (2D) Cd-bib coordination networks (Fig. 1b and S1a, ESI†). On the other hand, it was the two fluorine atoms on the *ortho*-position of SiF_6^{2-} anion that coordinated with Cd^{2+} cations to form one-dimensional (1D) zigzag coordination chains (Fig. 1c). In this regard, the Cd-bib networks were assembled by SiF_6^{2-} anions in the AB stacking mode to give the final 3D non-porous frameworks of complex **1** (Fig. 1d and S1b, ESI†), which is quite similar to the closed **SIFSIX-23-Cu** constructed from bib and $CuSiF_6$ reported by Zaworotko in 2020.[59]

Crystal structure of complex 2. According to the SC-XRD analysis, complex **2** was also crystallized in the monoclinic *C*2/*c* space group and its asymmetric unit contained two crystallographically independent half bib molecules, one-half Cd^{2+} cation, and one-half SiF_6^{2-} anion. Similar to complex **1**, the central cation Cd1 in complex **2** was also six-coordinated in a distorted octahedral coordination geometry surrounded by four nitrogen atoms (N1, N3, N1#1, N3#1) from four neighboring bib ligands and two fluorine atoms (F1, F1#1) from two SiF_6^{2-} anions (Fig. 2a). However, what was noteworthy is that one pair of the coordination plane of adjacent Cd^{2+} cations, which was defined by the four benzene ring centers coordinated with the same Cd^{2+} cation, was nearly vertical with the dihedral angle up to 84.83°, while another was parallel (Fig. S2a and b, ESI†). Therefore, the coordination between the ligand bib and Cd^{2+} cation formed 3D Cd-bib coordination networks (Fig. 2b). Meanwhile, due to the presence of ultralarge pores, the 3D Cd-bib networks were capable of intercrossing with the other two adjacent identical networks to minimize the porosity to stabilize the structure to form 3-fold interpenetrated Cd-bib coordination networks (Fig. 2c and S2c, ESI†). On the other hand, the SiF_6^{2-} anions in complex **2** were connected to Cd^{2+} cations by using the diagonal fluorine atoms to form 1D coordination chains (Fig. S2d, ESI†) and were inserted into the networks to assemble them into the final united coordination framework (Fig. 2d and S2e, ESI†). Despite the occurrence of interpenetration, there were still 1D channels along the *c*-axis with a size of *ca.* 3.5 × 5.0 Å in the structure of complex **2**,

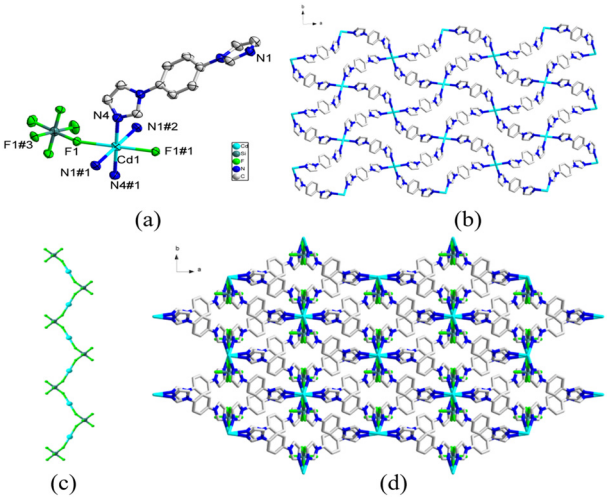

Fig. 1 (a) Coordination environment of Cd^{2+} in complex **1** with the ellipsoids drawn at the 50% probability level. The hydrogen atoms are omitted for clarity. Symmetry code: #1 −*x* + 1, −*y* + 1, −*z* + 1; #2 *x* − 1/2, −*y* + 1/2, *z* + 1/2; #3 −*x* + 3/2, *y* + 1/2, −*z* + 1/2. (b) Structure of the Cd-bib coordination networks along the *c*-axis and (c) 1D zigzag chain formed by the coordination of SiF_6^{2-} with Cd^{2+}. (d) The 3D framework structure of complex **1** along the *c*-axis.

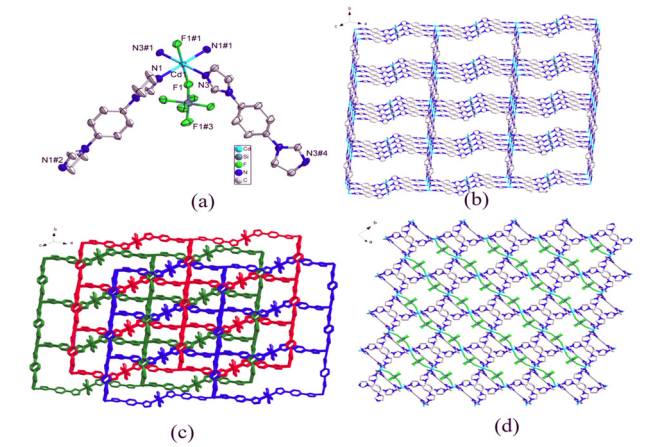

Fig. 2 (a) Coordination environment of Cd^{2+} in complex **2** with the ellipsoids drawn at the 50% probability level. The hydrogen atoms are omitted for clarity. Symmetry code: #1 −*x* + 1/2, −*y* + 1/2, −*z* + 1; #2 −*x* + 1, −*y* + 1, −*z* + 2; #3 −*x* + 1, *y*, −*z* + 3/2; #4 −*x* + 1, *y*, −*z* + 1/2. (b) Structure of the Cd-bib coordination networks. (c) The 3-fold interpenetrated Cd-bib networks. (d) The final 3D framework of complex **2** along the *c*-axis.

and the porosity was calculated to be 29.6% by using PLATON.[60] Although the coordination mode of the ligand bib with Cd^{2+} cation was quite similar between complexes **1** and **2**, the extension direction of the ligands coordinated with the neighboring Cd^{2+} cation and the coordination mode of SiF_6^{2-} with the Cd^{2+} cation led to a great difference in the structures of these two complexes.

Actually, Zaworotko and co-workers integrated the SiF_6^{2-} anion into the MOF $[Zn(bpy)_2(SiF_6)]_n{\cdot}x$DMF, by using $ZnSiF_6$ as the metal salt and 4,4′-bipyridine (bpy) as the ligand as early as 1995.[61] In this complex, the SiF_6^{2-} anion used the two F atoms at the *trans*-position to connect $[Zn(bpy)^2]_n$ grids into 3D frameworks with large square channels. Subsequently, some similar MOFs incorporating SiF_6^{2-} anions by using pyrazine or pyridine-based ligands to react with $MSiF_6$ (M = Co, Ni, Cu, Zn, Cd, *et al.*) have also been reported one after another.[62–68] In these complexes, almost all the SiF_6^{2-} anions in these MOFs adopted the *trans*-coordination configuration to connect the M-ligand chains or grids into 2D networks or 3D frameworks with 1D square channels, and the structure assembled by the connection of SiF_6^{2-} with interpenetrated networks has never been reported. All these results clearly show that the coordination mode of SiF_6^{2-} anions with the metal cations has a great effect on the structure and porosity of MOFs, and the *trans*-coordination mode makes it more possible to generate porous polymers.

PXRD, thermal stability, and morphology

PXRD measurements were carried out to examine the bulk-phase purity and structural consistency of the as-synthesized MOFs and the results are depicted in Fig. S3 (ESI†). It could be clearly observed that the PXRD patterns of the as-synthesized samples matched well with the simulated ones obtained from the SC-XRD data, demonstrating their phase purity and structural consistency. The thermal stability of these complexes was then studied by using TG analysis. As shown in Fig. S5 (ESI†), complex **1** displayed hardly any weight loss before 220 °C and a following obvious weight loss, which was in accordance with the results of the SC-XRD analysis and indicated it could maintain the framework up to 220 °C. Complex **2** exhibited a weight loss of 12.5% in the range of 30–240 °C corresponding to the release of the solvent DMF and water molecules (*ca.* 12.6%), and then its framework began to collapse up to 300 °C. Furthermore, it could be observed that compounds **1** and **2** possessed a layered microstructure in the SEM images (Fig. S6, ESI†).

Fluorescence sensing properties

Previous investigations have suggested that d^{10}-metal-based MOFs, such as Zn-MOF and Cd-MOF, usually exhibit distinct fluorescence properties and thus they have been extensively employed to construct fluorescence sensing materials. Hence, the fluorescence sensing properties of complexes **1** and **2** were investigated. Prior to the fluorescence sensing experiments, the crystalline samples of complexes **1** and **2** were fully ground and dispersed in deionized water ultrasonically to prepare steady suspensions (1.0 mg mL^{-1}). Then, their fluorescence excitation and emission bands were recorded at room temperature. As shown in Fig. S7 (ESI†), complexes **1** and **2** displayed a similar emission band with maxima at 309 and 310 nm upon excitation at 260 and 265 nm, respectively, and the similar fluorescence properties of complexes **1** and **2** may have originated from the same framework composition and coordination modes between bib and Cd^{2+}. In order to check their sensing capacity for amino acids, the fluorescence emission bands were collected after the addition of the solution of different amino acids (100 μL, 1 mM), including glycine (Gly), alanine (Ala), valine (Val), leucine (Leu), isoleucine (Ile), phenylalanine (Phe), tryptophan (Trp), tyrosine (Tyr), aspartic acid (Asp), asparagine (Asn), glutamic acid (Glu), lysine (Lys), glutamine (Gln), methionine (Met), serine (Ser), threonine (Thr), cysteine (Cys), proline (Pro), histidine (His), and arginine (Arg), into the suspensions of complexes **1** and **2**. As shown in Fig. 3a and b, it could be found that the fluorescence emission intensities of complexes **1** and **2** were both obviously enhanced upon the addition of Arg, while there were only slight or moderate changes in the emission intensities after the addition of the other amino acids, which indicated that complexes **1** and **2** could detect Arg selectively.

Subsequently, in order to check the sensing sensitivity of complexes **1** and **2** toward Arg, fluorescence titration experiments were conducted by the gradual addition of a solution of Arg into the suspensions of complexes **1** and **2**. As

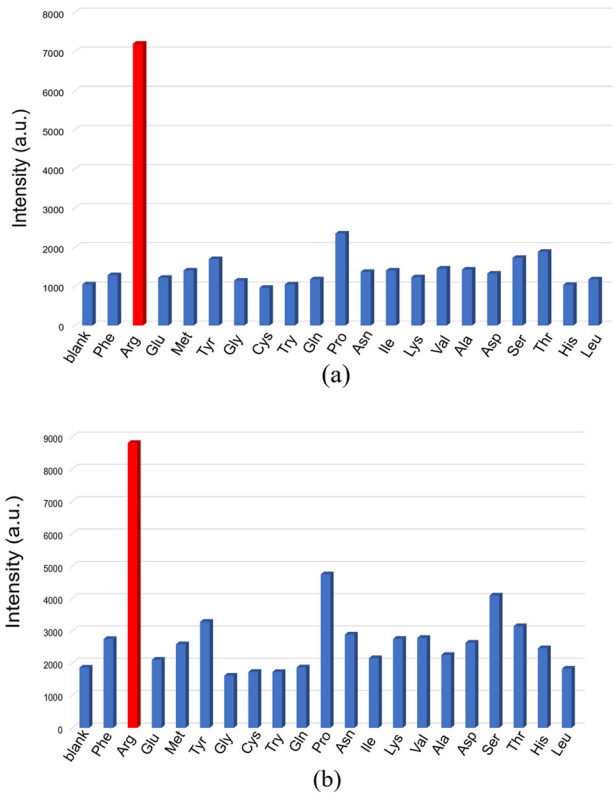

Fig. 3 Changes in the fluorescence emission intensities of complexes **1** (a) and **2** (b) after the addition of different amino acids.

exhibited in Fig. 4a and b, the emission intensities of complexes **1** and **2** continuously increased with the incremental addition of Arg, finally reaching up to 10.3 and 12.0 times the initial emission intensities, respectively. Furthermore, when the emission enhancement ratio I/I_0 against the concentration of Arg was plotted, where I_0 and I represent the emission intensities of the suspension of complexes **1** and **2** before and after the addition of Arg, it could be found that there was a linear relationship between them within the low concentration range with correlation coefficients (R^2) both higher than 0.99 (Fig. 4a and b), suggesting that complexes **1** and **2** may be used as quantitative sensors for Arg. According to the linear fitting results, the slopes were estimated to be 1.39×10^4 and 1.50×10^4 M^{-1} for complexes **1** and **2** respectively. Furthermore, the limit of detection (LOD) could be calculated by using the equation, LOD = $3\sigma/K$, where σ is the standard deviation and K is the slope, and the calculation results were 6.17×10^{-5} and 5.56×10^{-5} M for complexes **1** and **2**, respectively (Table S3, ESI†).

In consideration of practical applications, anti-interference and reusability are important and thus the anti-interfering and recycling performance of complexes **1** and **2** for the detection of Arg were examined. As shown in Fig. 5a and b, there were only slight or moderate changes in the emission intensities when the solutions of other interfering amino acids (100 μL,1 mM) were added into the suspensions of complexes **1** and **2**, but they were all significantly strengthened upon the addition of Arg, demonstrating that the presence of other amino acids had hardly any effect on the sensing capacity of complexes **1** and **2** toward Arg. After the sensing experiments, the samples of complexes **1** and **2** were collected by centrifugation, washed with water three times, and dried in an oven overnight. Then, the treated samples were dispersed in deionized water ultrasonically to prepare the steady suspensions of complexes **1** and **2** and these were then used to detect Arg again. As depicted in Fig. S8a and b (ESI†), complexes **1** and **2** were still capable of exhibiting a response to Arg *via* the "turn-on" effect, demonstrating their good reusability.

Finally, the sensing mechanism of complexes **1** and **2** toward Arg was considered as well. First, the structural destruction was taken into account and examined by PXRD experiments. As shown in Fig. S9 (ESI†), the PXRD patterns of complexes **1** and **2** after the sensing experiments remained nearly unchanged and matched well with the simulated ones, which clearly excluded the possibility of a structural collapse causing the emission enhancement. Furthermore, the UV-vis spectra revealed that there was hardly any absorption band in the range of 240–600 nm, which suggested there was no competitive

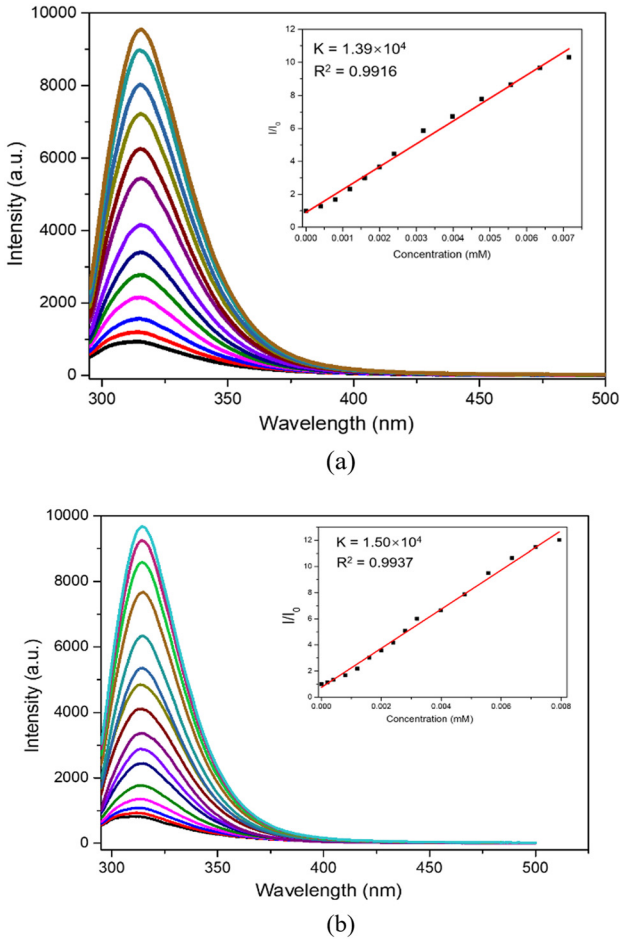

Fig. 4 Changes in the fluorescence emission of the aqueous suspensions of complexes **1** (a) and **2** (b) with the gradual addition of Arg. Inset: The plots of I/I_0 of the maximum intensities *versus* the concentration of Arg.

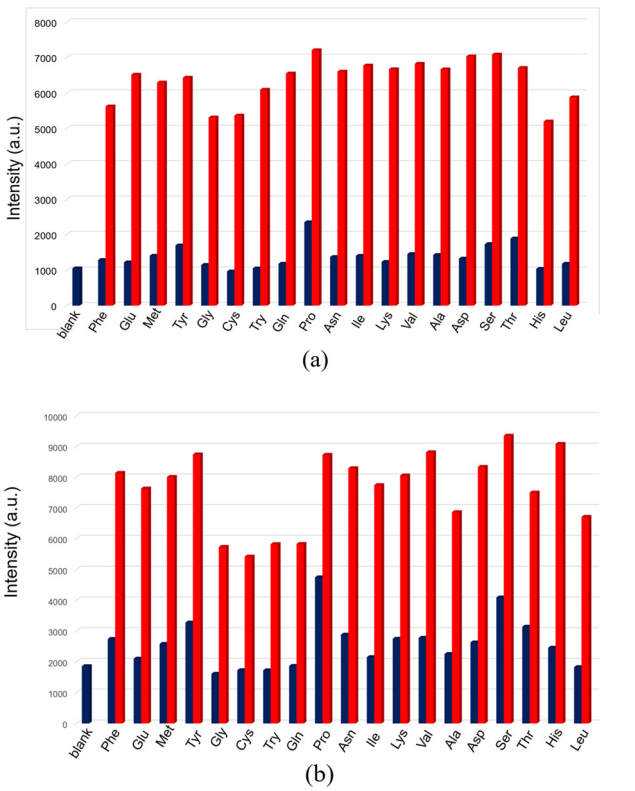

Fig. 5 Changes in the fluorescence intensities of complexes **1** (a) and **2** (b) after the successive addition of other interfering amino acids and Arg.

absorption between complexes **1** or **2** and Arg. On the other hand, in consideration of the fact that the emission bands of complexes **1** and **2** were red-shifted after the addition of Arg, we speculated that Arg may interact with the synthesized MOFs to cause changes in their fluorescence emission peaks. The FT-IR spectra of complexes **1** and **2** in the presence of Arg showed that the peaks of the Si–F stretching vibration around 935 cm^{-1}, C═N vibration around 1660 cm^{-1}, and C–H stretching vibration around 3120 cm^{-1} were weakened or shifted (Fig. S10, ESI†), which indicated the possible noncovalent interactions between complexes **1** or **2** and Arg, such as F···H–N, C═N···H, and C–H···N/O hydrogen interactions. Meanwhile, because Arg has the basic guanidine group that may be easily protonated to interact with synthesized complexes through electrostatic effects, the effect of guanidine hydrochloride on the fluorescence emission of complexes **1** and **2** was examined as well. As depicted in Fig. S11,† guanidine hydrochloride could obviously enhance the fluorescence emission of complexes **1** and **2**, indicating that the "turn-on" effect may be attributed to the interactions between the guanidine group of Arg and complexes **1** and **2**.

Conclusions

In summary, two novel Cd(II)-based MOFs were successfully synthesized by the reaction of an imidazole-containing ligand and $CdSiF_6$. According to the SC-XRD results, although these two compounds possessed the same framework composition without regard to the solvents, they exhibited completely different structures. Complex **1** was a non-porous 3D coordination framework built from Cd-bib layers and SiF_6^{2-} anions, while complex **2** displayed a porous 3D coordination architecture constituted by 3-fold interpenetrated Cd-bib networks and SiF_6^{2-} anions. The differences in their structure could be attributed to the extension direction of the ligands coordinated with the neighboring Cd^{2+} cation and the coordination mode of SiF_6^{2-} with the Cd^{2+} cation. Furthermore, the fluorescence emission intensities of complexes **1** and **2** increased up to 10.3 and 12.0 times that of the initial emission intensities upon the addition of Arg. Thus, complexes **1** and **2** could be used as "turn-on" fluorescent sensors for Arg and they also showed high selectivity, anti-interfering capability, and reusability. The synthesized MOF-based probes may provide a convenient detection platform for related research on arginine in tumors and immunity.

Conflicts of interest

There are no conflicts of interest to declare.

Acknowledgements

We acknowledge the National Natural Science Foundation of China (grant no. 21401099, 22025701 and 91753121) and the Shenzhen Basic Research Program (JCYJ20180508182240106).

References

1 Y. Sancak, T. R. Peterson, Y. D. Shaul, R. A. Lindquist, C. C. Thoreen, L. Bar-Peled and D. M. Sabatini, *Science*, 2008, **320**, 1496–1501.
2 C. J. Accardi, D. I. Walker, K. Uppal, A. A. Quyyumi, P. Rohrbeck, K. D. Pennell, C. T. M. Mallon and D. P. Jones, *J. Occup. Environ. Med.*, 2016, **58**, 80–88.
3 R. Dalangin, A. Kim and R. E. Campbell, *Int. J. Mol. Sci.*, 2020, **21**, 6197.
4 L. S. Lundell, E. B. Parr, B. L. Devlin, L. R. Ingerslev, A. Altıntaş, S. Sato, P. Sassone-Corsi, R. Barrès, J. R. Zierath and J. A. Hawley, *Nat. Commun.*, 2020, **11**, 4643.
5 D. de la Torre and J. W. Chin, *Nat. Rev. Genet.*, 2021, **22**, 169–184.
6 R. Ravindran, J. Loebbermann, H. I. Nakaya, N. Khan, H. Ma, L. Gama, D. K. Machiah, B. Lawson, P. Hakimpour, Y. C. Wang, S. Li, P. Sharma, R. J. Kaufman, J. Martinez and B. Pulendran, *Nature*, 2016, **531**, 523–527.
7 P. Jouandin, Z. Marelja, Y. H. Shih, A. A. Parkhitko, M. Dambowsky, J. M. Asara, I. Nemazanyy, C. C. Dibble, M. Simons and N. Perrimon, *Science*, 2022, **375**, eabc4203.
8 F. Püschel, F. Favaro, J. Redondo-Pedraza, E. Lucendo, R. Iurlaro, S. Marchetti, B. Majem, E. Eldering, E. Nadal, J. E. Ricci, E. Chevet and C. Muñoz-Pinedo, *Proc. Natl. Acad. Sci. U. S. A.*, 2020, **117**, 9932–9941.
9 M. Tajan, M. Hennequart, E. C. Cheung, F. Zani, A. K. Hock, N. Legrave, O. D. K. Maddocks, R. A. Ridgway, D. Athineos, A. Suárez-Bonnet, R. L. Ludwig, L. Novellasdemunt, N. Angelis, V. S. W. Li, G. Vlachogiannis, N. Valeri, N. Mainolfi, V. Suri, A. Friedman, M. Manfredi, K. Blyth, O. J. Sansom and K. H. Vousden, *Nat. Commun.*, 2021, **12**, 366.
10 S. C. Hsu, C. L. Chen, M. L. Cheng, C. Y. Chu, G. C. A. Chan, Y. L. Yu, S. D. Yeh, T. C. Kuo, C. C. Kuo, C. P. Chuu, C. F. Li, L. H. Wang, H. W. Chen, Y. Yen, D. K. Ann, H. J. Wang and H. J. Kung, *Theranostics*, 2021, **11**, 7527–7545.
11 K. Tang, H. Zhang, J. Deng, D. Wang, S. Liu, S. Lu, Q. Cui, C. Chen, J. Liu, Z. Yang, Y. Li, J. Chen, J. Lv, J. Ma and B. Huang, *Nat. Immunol.*, 2023, **24**, 162–173.
12 F. Halperin, T. Mezza, P. Li, J. Shirakawa, R. N. Kulkarni and A. B. Goldfine, *Metabolism*, 2022, **128**, 155117.
13 A. T. Singh and F. R. Causland, *Semin. Dial.*, 2017, **30**, 509–517.
14 T. M. Grzywa, A. Sosnowska, P. Matryba, Z. Rydzynska, M. Jasinski, D. Nowis and J. Golab, *Front. Immunol.*, 2020, **11**, 938.
15 S. M. Morris, *Annu. Rev. Nutr.*, 2002, **22**, 87–105.
16 D. Liebsch, M. Juvany, Z. Li, H. L. Wang, A. Ziolkowska, D. Chrobok, C. Boussardon, X. Wen, S. R. Law, H. Janečková, B. Brouwer, P. Lindén, N. Delhomme, H. Stenlund, T. Moritz, P. Gardeström, H. Guo and O. Keech, *Plant Physiol.*, 2022, **189**, 1943–1960.
17 R. M. Palmer, *Curr. Opin. Nephrol. Hypertens.*, 1993, **2**, 122–128.
18 S. M. Morris, *J. Nutr.*, 2016, **146**, 2579–2586.
19 N. M. Kanaan, G. Morfini, G. Pigino, N. E. LaPointe, A. Andreadis, Y. Song, E. Leitman, L. I. Binder and S. T. Brady, *Neurobiol. Aging*, 2012, **33**, 15–30.

20 F. Niu, Y. Yu, Z. Li, Y. Ren, Z. Li, Q. Ye, P. Liu, C. Ji, L. Qian and Y. Xiong, *Biomed. Pharmacother.*, 2022, **149**, 112840.
21 K. Hermann, C. E. von Eschenbach, M. von Tschirschnitz and J. Ring, *Regul. Pept.*, 1993, **49**, 1–7.
22 P. C. Colombani, R. Bitzi, P. Frey-Rindova, W. Frey, M. Arnold, W. Langhans and C. Wenk, *Eur. J. Nutr.*, 1999, **38**, 263–270.
23 Z. Melik, P. Zaletel, T. Virtic and K. Cankar, *Clin. Hemorheol. Microcirc.*, 2017, **65**, 205–217.
24 A. Khurana, M. A. Saifi and C. Godugu, *Biol. Trace Elem. Res.*, 2023, **201**, 3404–3417.
25 J. Xu and S. Richard, *Mol. Cell*, 2021, **81**, 4357–4368.
26 S. Y. Liao, M. R. Showalter, A. L. Linderholm, L. Franzi, C. Kivler, Y. Li, M. R. Sa, Z. A. Kons, O. Fiehn, L. Qi, A. A. Zeki and N. J. Kenyon, *JCI Insight*, 2020, **5**, e137777.
27 D. Zakrzewicz and O. Eickelberg, *BMC Pulm. Med.*, 2009, **9**, 5.
28 C. L. Chen, S. C. Hsu, T. Y. Chung, C. Y. Chu, H. J. Wang, P. W. Hsiao, S. D. Yeh, D. K. Ann, Y. Yen and H. J. Kung, *Nat. Commun.*, 2021, **12**, 2398.
29 S. Alessandra, G. Grassi, S. Notari, S. Gili, V. Bordoni, E. Tartaglia, R. Casetti, E. Cimini, D. Mariotti, G. Garotto, A. Beccacece, L. Marchioni, M. Bibas, E. Nicastri, G. Ippolito and C. Agrati, *Cell*, 2021, **10**(8), 2111.
30 Q. Wang, M. A. Priestman and D. S. Lawrence, *Angew. Chem., Int. Ed.*, 2013, **52**, 2323–2325.
31 J. Martens-Lobenhoffer and S. M. Bode-Böger, *J. Chromatogr., B*, 2003, **798**, 231–239.
32 P. S. Francis, J. L. Adcock, J. W. Costin and K. M. Agg, *Anal. Biochem.*, 2005, **336**, 141–143.
33 G. Paglia, O. D'Apolito, F. Tricarico, D. Garofalo and G. Corso, *J. Sep. Sci.*, 2008, **31**, 2424–2429.
34 A. Barilli, R. Visigalli, B. M. Rotoli, O. Bussolati, G. C. Gazzola, A. Parolari and V. Dall'Asta, *Anal. Biochem.*, 2012, **424**, 156–161.
35 X. H. Liu, J. G. Ma, Z. Niu, G. M. Yang and P. Cheng, *Angew. Chem., Int. Ed.*, 2015, **54**, 988–991.
36 M. Eddaoudi, D. F. Sava, J. F. Eubank, K. Adil and V. Guillerm, *Chem. Soc. Rev.*, 2015, **44**, 228–249.
37 Z. Hu, B. J. Deibert and J. Li, *Chem. Soc. Rev.*, 2014, **43**, 5815–5840.
38 J. R. Li, R. J. Kuppler and H. C. Zhou, *Chem. Soc. Rev.*, 2009, **38**, 1477–1504.
39 H. Furukawa, K. E. Cordova, M. O'Keeffe and O. M. Yaghi, *Science*, 2013, **341**, 1230444.
40 W. P. Lustig, S. Mukherjee, N. D. Rudd, A. V. Desai, J. Li and S. K. Ghosh, *Chem. Soc. Rev.*, 2017, **46**, 3242–3285.
41 J. Meng, X. Liu, C. Niu, Q. Pang, J. Li, F. Liu, Z. Liu and L. Mai, *Chem. Soc. Rev.*, 2020, **49**, 3142–3186.
42 F. Yan, X. Wang, Y. Wang, C. Yi, M. Xu and J. Xu, *Microchim. Acta*, 2022, **189**, 379.
43 N. Wang, Y. Wu, M. Wang, Z. Li, G. Wang and X. Su, *Analyst*, 2021, **146**, 5280–5286.
44 X. Wang, Y. Zhang, Z. Shi, T. Lu, Q. Wang and B. Li, *ACS Appl. Mater. Interfaces*, 2021, **13**, 54217–54226.
45 T. He, X. J. Kong and J. R. Li, *Acc. Chem. Res.*, 2021, **54**, 3083–3094.
46 S. Bej and P. Banerjee, *Spectrochim. Acta, Part A*, 2022, **283**, 121764.
47 M. Kaur, S. K. Mehta and S. K. Kansal, *Environ. Sci. Pollut. Res.*, 2023, **30**, 8464–8484.
48 H. Q. Yin, X. Y. Wang and X. B. Yin, *J. Am. Chem. Soc.*, 2019, **141**, 15166–15173.
49 J. J. Hu, Y. G. Li, H. R. Wen, S. J. Liu, Y. Peng and C. M. Liu, *Inorg. Chem.*, 2022, **61**, 6819–6828.
50 L. Wang, B. Tu, W. Xu, Y. Fu and Y. Zheng, *Inorg. Chem.*, 2020, **59**, 5004–5017.
51 S. Senthilkumar, R. Goswami, V. J. Smith, H. C. Bajaj and S. Neogi, *ACS Sustainable Chem. Eng.*, 2018, **6**, 10295–10306.
52 Y. Xiao, Y. Wang, Z. X. You, Q. L. Guan, Y. H. Xing, F. Y. Bai and L. X. Sun, *Cryst. Growth Des.*, 2022, **22**, 6967–6976.
53 A. Mandal, A. Adhikary, A. Sarkar and D. Das, *Inorg. Chem.*, 2020, **59**, 17758–17765.
54 E. Peris, *Chem. Rev.*, 2018, **118**, 9988–10031.
55 S. S. Chen, Z. Y. Zhang, R. B. Liao, Y. Zhao, C. Wang, R. Qiao and Z. D. Liu, *Inorg. Chem.*, 2021, **60**, 4945–4956.
56 Y. Li, Y. Y. An, J. Z. Fan, X. X. Liu, X. Li, F. E. Hahn, Y. Y. Wang and Y. F. Han, *Angew. Chem., Int. Ed.*, 2020, **59**, 10073–10080.
57 Y. W. Zhang, S. Bai, Y. Y. Wang and Y. F. Han, *J. Am. Chem. Soc.*, 2020, **142**, 13614–13621.
58 Q. Chu, Z. Su, J. Fan, T. Okamura, G. C. Chao Lv, G. X. Liu, W. Y. Sun and N. Ueyama, *Cryst. Growth Des.*, 2011, **11**, 3885–3894.
59 B. Q. Song, Q. Y. Yang, S. Q. Wang, M. Vandichel, A. Kumar, C. Crowley, N. Kumar, C. H. Deng, V. GasconPerez, M. Lusi, H. Wu, W. Zhou and M. J. Zaworotko, *J. Am. Chem. Soc.*, 2020, **142**, 6896–6901.
60 A. L. Spek, *J. Appl. Crystallogr.*, 2003, **36**, 7–13.
61 S. Subramanian and M. J. Zaworotko, *Angew. Chem., Int. Ed. Engl.*, 1995, **34**, 2127–2129.
62 K. Emura, A. Maeda, T. K. Maji, P. Kanoo and H. Kita, *Eur. J. Inorg. Chem.*, 2009, 2329–2337.
63 M. J. Lin, A. Jouaiti, N. Kyritsakas and M. W. Hosseini, *CrystEngComm*, 2011, **13**, 776–778.
64 O. Alduhaish, R.-B. Lin, H. L. Wang, B. Li, H. D. Arman, T.-L. Hu and B. L. Chen, *Cryst. Growth Des.*, 2018, **18**, 4522–4527.
65 J. J. Liu, Y. J. Hong, Y. F. Guan, M. J. Lin, C. C. Huang and W. X. Dai, *Dalton Trans.*, 2015, **44**, 653–658.
66 M. J. Lin, A. Jouaiti, D. Pocic, N. Kyritsakas, J.-M. Planeix and M. W. Hosseini, *Chem. Commun.*, 2010, **46**, 112–114.
67 A. Bajpai, M. Lusi and M. J. Zaworotko, *Chem. Commun.*, 2017, **63**, 3978–3981.
68 R. B. Lin, L. B. Li, H. Wu, H. Arman, B. Li, R. G. Lin, W. Zhou and B. L. Chen, *J. Am. Chem. Soc.*, 2017, **139**, 8022–8028.